Chemical Physics 110 (1986) 375–389
North-Holland, Amsterdam

INTRAMOLECULAR DYNAMICS BY PHOTOELECTRON SPECTROSCOPY. III. PREDISSOCIATION OF THE $\tilde{B}\,^2B_2$ STATE OF H_2O^+ AND D_2O^+ BY A SEMICLASSICAL APPROACH

Dominique DEHARENG

Département de Chimie, Université de Liège, Sart-Tilman, B-4000 Liège 1, Belgium

Received 30 June 1986

The initial wave packets of H_2O^+ and D_2O^+ in their $\tilde{B}\,^2B_2/^2A'$ states are expanded in the frozen gaussian basis set proposed by Heller. The gaussian functions are propagated on the adiabatic and diabatic potential energy surfaces resulting from the conical intersection with the $\tilde{A}\,^2A_1/^2A'$ state. Autocorrelation functions are calculated separately for the adiabatic and diabatic motions of the nuclei. These autocorrelation functions are compared with their experimental counterparts. The agreement is qualitatively good and the isotope effects are well accounted for.

1. Introduction

The autocorrelation function provides an interesting piece of information on the nuclear motion on the potential energy surface of the electronic state under consideration and has already proven its usefulness [1–3] for the understanding of the intramolecular dynamics. In this paper, we use the method of frozen gaussians proposed by Heller [4] to calculate the autocorrelation function $C(t)$ corresponding to the $\tilde{B}\,^2A'$ state of H_2O^+ and D_2O^+. Such a semiclassical treatment already provided good results for a diatomic system [5] and can also be used for polyatomic systems [6].

The purpose of this work is to explain the isotope effect observed in the experimental autocorrelation functions of H_2O^+ and D_2O^+ in their $\tilde{B}\,^2B_2/^2A'$ state, particularly in the region corresponding to the second recurrence ($800 \lesssim t \lesssim 1100$ au for H_2O^+ and $1100 \lesssim t \lesssim 1600$ au for D_2O^+) (fig. 1, solid line). The case of the $\tilde{B}\,^2A'$ state of H_2O^+ (D_2O^+) is particularly exemplary since this state is connected with the $\tilde{A}\,^2A'$ state via a conical intersection [7–9]. Whether the calculated and experimental autocorrelation functions (the latter being obtained by Fourier transforming the band profile of the photoelectron spectrum [10]) have similar shapes and present the same important features will be indicative of the validity of the model used to describe the dynamical behavior of the system. In section 2, we present the adiabatic

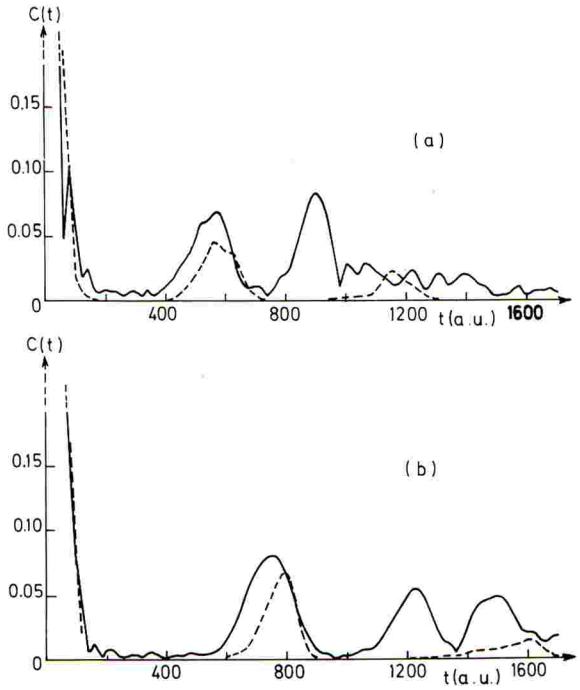

Fig. 1. Solid line: experimental autocorrelation functions; dashed line: calculated adiabatic autocorrelation functions. (a) H_2O^+ ($\tilde{B}\,^2A'$ state). (b) D_2O^+ ($\tilde{B}\,^2A'$ state).

and diabatic potential energy surfaces used for the trajectory calculation of the gaussians' motion and we briefly indicate how we calculate the transition probability. Section 3 deals with the choice of the initial conditions for the trajectories and the determination of the initial wavefunction. In section 4, the gaussian basis set is presented and the expression for $C(t)$ is derived. This analytical expression can only be obtained in the case where the determinant of the metric tensor **g** for the chosen coordinates is constant. If this is not the case, one has to look for more appropriate coordinates. This transformation is carried out in section 5. Section 6 deals with the choice of the width of the gaussian functions of the basis set. This width must be determined so as to minimize the error due to the frozen character of the gaussians. In section 7, we present the results, discuss the agreement with the experimental autocorrelation function and we comment on the isotope effect observed. Section 8 provides a more general discussion and interpretation of the results.

2. Potential energy surfaces and transition probability

The conical intersection between the $\tilde{A}$ and $\tilde{B}\,^2A'$ states of X_2O^+ (X = H or D) is schematically presented in fig. 2. The coordinates (R, r, α) are defined as follows. Let the bond lengths be $R_1 = OX_1$, $R_2 = X_1X_2$, $R_3 = OX_2$,

$R = \frac{1}{2}(R_1 + R_3)$,

$r = R_3 - R_1$,

α is the angle between R_1 and R_3.

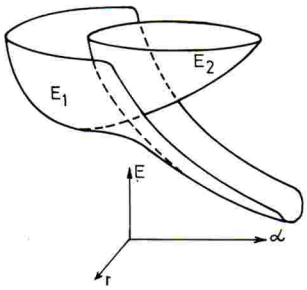

Fig. 2. Perspective drawing of the $\tilde{B}\,^2A'$ and $\tilde{A}\,^2A'$ adiabatic potential energy surfaces.

In a previous study the adiabatic potential energy surfaces were calculated ab initio and a dynamical study of the relaxation process from the $\tilde{B}$ to the $\tilde{A}$ state was presented [8,9]. This study was based on classical trajectory calculations on the upper adiabatic surface interpolated by the 3D spline method [11]. For each trajectory, a non-adiabatic transition probability was calculated by the Nikitin two-dimensional formula [12] every time the trajectory passes through a "seam" $\alpha_c = f(R)$. This seam is a line within the region of strong coupling between the two adiabatic states and is taken as being the locus of the apex of the double cone. The final transition probability was obtained by averaging over the ensemble of trajectories. This led to a rate constant for the depopulation of the $\tilde{B}$ state of the order of 10^{14} s^{-1}.

In order to obtain the autocorrelation function, we must also consider the evolution of the part of the wavefunction that does not remain on the upper adiabatic surface. In the region of non-adiabatic interaction, the wave packet breaks into two parts (fig. 3). Beyond the coupling zone, the first one (WP1) has remained on the upper adiabatic surface while the second (WP2) has dropped down on the lower one. The potential which

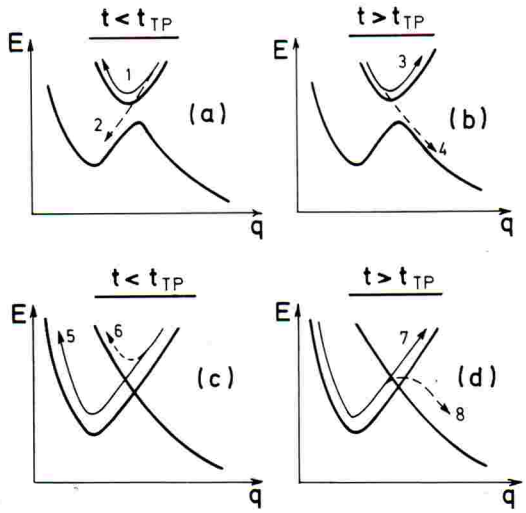

Fig. 3. Schematic views of the adiabatic and diabatic trajectory flows, before and after the turning point time t_{TP}. Solid line: calculated flux; dashed line: neglected flux. (a) and (b): calculation on the upper adiabatic potential energy surface; (c) and (d): calculation on the diabatic potential energy surface.

governs the motion of WP1 is already known [8,9] and results from a 3D spline interpolation. The potential in which WP2 moves is taken as the diabatic energy surface which coincides with the upper adiabatic surface in the Franck–Condon region and with the lower one after the passage through the coupling zone. As discussed by several authors [13], true diabatic states do not in general exist. However, under certain conditions [14], satisfactory approximate diabatic states can be derived. It seems that the conical intersection under study can be classified in the favourable cases and diabatic potential energies have already been calculated [8,9]. The surface obtained corresponds to H_{11} in fig. 4.

We preferred to consider a model in which the motion of WP2 is continuous on an approximate diabatic potential than to use a surface hopping model in which the velocities have to be corrected at each hop to the lower adiabatic surface. This approximate diabatic state is known at few points only (120–150). These points are introduced as input data in the program POT3 ☆. The expression for the derived potential was originally suggested by Sorbie and Murrell [16] and later extended by Murrell et al. [17], based on the many-body expansion:

$$V(R_1, R_2, R_3) = \sum_i V_i^{(1)} + \sum_i V_i^{(2)}(R_i) + V^{(3)}(R_1, R_2, R_3). \quad (1)$$

$V(R_1, R_2, R_3)$ is the required total energy of the triatom relative to the combined ground state energies of the atoms 1, 2 and 3. $V_i^{(1)}$ are atomic energies relative to the ground states, $V_i^{(2)}(R_i)$ are two-body interaction terms relative to dissociated atoms and $V^{(3)}(R_1, R_2, R_3)$ is a three-body interaction term. $V_i^{(1)}$ and $V_i^{(2)}(R_i)$ have to be introduced as input data and the program POT3 determines $V^{(3)}(R_1, R_2, R_3)$ with the help of ab initio energies and the requirement that the minimum of the surface be exactly reproduced.

☆ Program POT3 [15] is a standard FORTRAN IV computer program developed at the University of Reading for the purpose of deriving analytical triatomic potential functions which reproduce spectroscopic, thermochemical, ab initio or kinetic data.

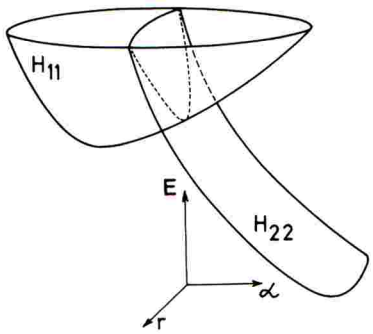

Fig. 4. Perspective drawing of the $\tilde{B}$ and $\tilde{A}$ states in the diabatic representation. The seam is represented by a dotted line.

In the study of the diabatic motion of the wave packet, each trajectory moves on this potential energy surface and every time it crosses the locus $\alpha_C = f(R)$ the probability of switching is calculated [8,9] from the Nikitin formula [12]. Thus, the dynamical behavior on the diabatic potential energy surface is treated at the same level as that on the adiabatic one; the probabilities p_i are calculated by the same formula, except that p_i in one picture becomes $(1 - p_i)$ in the other. Thus, the motions of WP1 and WP2 are confined to single potential energy surfaces but the loss of flux is accounted for.

3. Initial conditions and initial state

The initial conditions are denoted $\{R_i^{in}, r_i^{in}, \alpha_i^{in}, \phi_i^{in}, \theta_i^{in}, \chi_i^{in}, p_{R_i}^{in}, p_{r_i}^{in}, p_{\alpha_i}^{in}, p_{\phi_i}^{in}, p_{\theta_i}^{in}, p_{\chi_i}^{in}\}$, where $\{R_i^{in}, r_i^{in}, \alpha_i^{in}\}$ represents the initial values of the internal coordinates for the ith trajectory, $\{\phi_i^{in}, \theta_i^{in}, \chi_i^{in}\}$ represents the initial values of the Euler angles for the ith trajectory, and the p_i^{in} represent the initial values of the conjugate momenta for the ith trajectory. The choice of the initial conditions $\{R_i^{in}, r_i^{in}, \alpha_i^{in}, p_{R_i}^{in}, p_{r_i}^{in}, p_{\alpha_i}^{in}\}$ is based on the value of their statistical weights. These are taken as the values of the Wigner function [18] at the corresponding values of the normal coordinates and conjugate momenta $\{Q_{1i}^{in}, Q_{2i}^{in}, Q_{3i}^{in}, P_{1i}^{in}, P_{2i}^{in}, P_{3i}^{in}\}$ whose relationship with the internal coordinates is given in refs. [8,9]. As the number of trajectories which can be run is limited,

we choose among a set of randomly generated initial conditions those with the highest statistical weight. The signs of the conjugate momenta were randomly chosen.

The initial orientation of the molecule in space does not matter and the initial values of the Euler angles are taken the same for all the trajectories. The initial values of the conjugate momenta $\{ p_{\phi_i}^{\text{in}}, p_{\theta_i}^{\text{in}}, p_{\chi_i}^{\text{in}} \}$ are randomly generated for a given rotational quantum number J [8,9].

The initial nuclear wavefunction corresponds to the potential of the $H_2O(\tilde{X}\,{}^1A'')$ molecule in the harmonic approximation:

$$\Psi_0 = N \exp\left(-\frac{1}{2\hbar} \sum_{i=1}^{3} \omega_i Q_i^2 \right), \tag{2}$$

where ω_i is the pulsation of the ith normal mode. They are derived from the valence force field of Bartlett et al. [19].

As the internal coordinates used (R, r, α) are not cartesian, relation (2) becomes

$$\Psi_0 = N \exp\left[-(1/2\hbar)(\boldsymbol{q} - \boldsymbol{q}_e)^{\mathrm{T}} \cdot \mathbf{A} (\boldsymbol{q} - \boldsymbol{q}_e) \right], \tag{3}$$

with

$$\boldsymbol{q} - \boldsymbol{q}_e = \begin{pmatrix} R - R_e \\ r - r_e \\ \alpha - \alpha_e \end{pmatrix},$$

R_e, r_e, α_e are the equilibrium values for the molecule. The elements of matrix $\mathbf{A}$ are obtained from the ω_i and the relations between ($R - R_e$, $r - r_e$, $\alpha - \alpha_e$) and (Q_1, Q_2, Q_3) [8,9]. The normalization factor N is given by

$$N = \left(\prod_{i=1}^{3} \omega_i / \pi^3 \hbar^3 \right)^{1/4} = \left(\det \mathbf{A} / \pi^3 \hbar^3 g \right)^{1/4}, \tag{4}$$

if the determinant g of the metric tensor $\mathbf{g}$ is constant.

4. Gaussian basis set and expression for $C(t)$

The method used in this work has been proposed by Heller [4] and consists in the expansion of the nuclear wavefunction $\Psi(\boldsymbol{q}, t)$ in a basis of frozen gaussian functions $G_j(\boldsymbol{q}, t)$ [6]:

$$\Psi(\boldsymbol{q}, t) = \sum_{j=1}^{N} c_j G_j(\boldsymbol{q}, t), \tag{5}$$

$$G_j(\boldsymbol{q}, t) = N' \exp\left\{ -(1/2\hbar)\left[\boldsymbol{q} - \boldsymbol{q}_j(t)\right]^{\mathrm{T}} \cdot \mathbf{B}\left[\boldsymbol{q} - \boldsymbol{q}_j(t)\right] + (\mathrm{i}/\hbar)\boldsymbol{p}_j(t)^{\mathrm{T}} \cdot \left[\boldsymbol{q} - \boldsymbol{q}_j(t)\right] + (\mathrm{i}/\hbar)\gamma_j(t) \right\}, \tag{6}$$

where $(\boldsymbol{q}_j(t), \boldsymbol{p}_j(t))$ are the vectors of the internal coordinates and conjugate momenta that obey the classical equations of motion. The phase $\gamma_j(t)$ is given by

$$\gamma_j(t) = \int_0^t \left[\boldsymbol{p}_j(t')^{\mathrm{T}} \cdot \dot{\boldsymbol{q}}(t') - E_j \right] \mathrm{d}t', \tag{7}$$

where E_j is the classical total energy of the jth trajectory.

$$N' = \left(\det \mathbf{B} / g\pi^3\hbar^3 \right)^{1/4},$$

if the determinant g is constant. The matrix $\mathbf{B}$ is held constant and its choice is discussed in section 6.

For the determination of the values of the c_j coefficients in relation (5), one has to remember that the gaussian functions as given by eq. (6) are not orthogonal. Diagonalization of the overlap matrix [20]

$$S_{ij} = \iiint_{-\infty}^{\infty} \left(g^{1/2}\, \mathrm{d}\boldsymbol{q} \right) \boldsymbol{G}_i^*(\boldsymbol{q}, 0)\, G_j(\boldsymbol{q}, 0), \tag{8}$$

leads to a new basis set of orthogonal functions $F_i(\boldsymbol{q}, 0)$

$$F_i(\boldsymbol{q}, 0) = \sum_{j=1}^{N} f_{ij} G_j(\boldsymbol{q}, 0). \tag{9}$$

The wavefunction $\Psi(\boldsymbol{q}, t)$ is expanded in the $P \leqslant N$ linearly independent basis functions $F_i(\boldsymbol{q}, t)$ [20]

$$\Psi(\boldsymbol{q}, t) = \sum_{i=1}^{P} u_i F_i(\boldsymbol{q}, t) = \sum_{j=1}^{N} c_j G_j(\boldsymbol{q}, t), \tag{10}$$

$$c_j = \sum_{i=1}^{P} u_i f_{ij}, \tag{11}$$

$$u_i = \left[\sum_{j=1}^{N} f_{ij}^{*} \iiint_{-\infty}^{\infty} (g^{1/2}\, \mathrm{d}\boldsymbol{q})\, G_j^{*}(\boldsymbol{q}, 0)\, \Psi_0 \right] \left[\iiint_{-\infty}^{\infty} (g^{1/2}\, \mathrm{d}\boldsymbol{q}) \mid F_i(\boldsymbol{q}, 0) \mid^2 \right]^{-1}. \tag{12}$$

These integrals are of the same type as S_{ij} [eq. (8)]. The general expression for S_{ij} is given in the appendix. As pointed out there, a general analytical expression for S_{ij} exists only when $g^{1/2}$ is constant and can be moved out of the integration symbol. Otherwise, the three-dimensional integrals must be calculated numerically. The autocorrelation function takes the form

$$\begin{aligned} C(t) &= \left| \iiint_{-\infty}^{\infty} (g^{1/2}\, \mathrm{d}\boldsymbol{q}) \Psi^{*}(\boldsymbol{q}, 0) \Psi(\boldsymbol{q}, t) \right| \\ &= \Bigg| \sum_i \sum_j c_i c_j^{*} P_i^{1/2}(t) \exp\Big\{ -(1/4\hbar) \big[\boldsymbol{q}_i(t) - \boldsymbol{q}_j(0)\big]^{\mathrm{T}} \cdot \mathbf{B} \big[\boldsymbol{q}_i(t) - \boldsymbol{q}_j(0)\big] \\ &\quad - (1/4\hbar) \big[\boldsymbol{p}_i(t) - \boldsymbol{p}_j(0)\big]^{\mathrm{T}} \cdot \mathbf{B}^{-1} \big[\boldsymbol{p}_i(t) - \boldsymbol{p}_j(0)\big] \\ &\quad + (i/\hbar) \Big\{ \boldsymbol{p}_j(0)^{\mathrm{T}} \cdot \boldsymbol{q}_j(0) - \boldsymbol{p}_i(t)^{\mathrm{T}} \cdot \boldsymbol{q}_i(t) + \big[\boldsymbol{p}_i(t) - \boldsymbol{p}_j(0)\big]^{\mathrm{T}} \cdot \boldsymbol{Q}_{ji} + \gamma_i(t) \Big\} + K \Big\} \Bigg|, \end{aligned} \tag{13}$$

where $P_i(t)$ is the probability for the ith trajectory $(\boldsymbol{q}_i(t), \boldsymbol{p}_i(t))$ of remaining on the potential energy surface on which the wave packet moves. The probability amplitude of remaining on the potential energy surface associated with the trajectory $(\boldsymbol{q}_i(t), \boldsymbol{p}_i(t))$ is characterized by its absolute value and its phase. In the model adopted here, we choose to neglect the phase and we take $P_i^{1/2}(t)$ as the probability amplitude associated with the gaussian $G_i(\boldsymbol{q}, t)$. $\boldsymbol{Q}_{ji}$ and K are given in the appendix.

The reason why we do not consider any interference between the adiabatic and diabatic wave packets is the following. According to the results of refs. [8,9], that part of the wave packet which remains on the upper adiabatic potential energy surface is small ($\approx 10\%$ or less). We made the assumption that the part of the autocorrelation function due to interference effects should be still lower than the adiabatic function and could be neglected. The results obtained seem to indicate that this assumption is acceptable. In the case where the wave packet breaks into two similar wave packets on each surface, this assumption is probably no longer valid.

5. Coordinate transformation

For the coordinates (R, r, α), the determinant of the metric tensor has the following expression

$$g = \tfrac{1}{2}(1 - 2\gamma) \big\{ R^2 \big[1 - 2\gamma \sin^2(\alpha/2)\big] + \tfrac{1}{4} r^2 \big[1 - 2\gamma \cos^2(\alpha/2)\big] \big\}, \tag{14}$$

where

$$\gamma = m_{\mathrm{X}}/(m_0 + 2m_{\mathrm{X}}) \quad (\mathrm{X} = \mathrm{H} \text{ or } \mathrm{D}).$$

As mentioned above, if one wants to calculate

$C(t)$ by relation (13), one has to choose a coordinate system for which g is constant. This is the case for the system given in fig. 5. The new axis y passes through the center of mass G of the triatom and the center of mass M of the diatom X_1–X_2. G is the origin of the new body-fixed frame. The new coordinates are defined as follows (fig. 5):

$$R_4 = y_{X_1} - y_O,$$
$$R_O = y_M - y_O,$$
$$R_5 = x_{X_2}. \tag{15}$$

In this coordinate system, the vibrational kinetic energy T_{shape} [21] and the determinant g are given by

$$T_{shape} = [2m_X(m_O + m_X)/(m_O + 2m_X)]\,\dot{R}_O^2 + m_X(\dot{R}_4^2 + \dot{R}_5^2) - 2m_X\dot{R}_4\dot{R}_O, \tag{16}$$

$$g = 8m_X^3 m_O/(2m_X + m_O). \tag{17}$$

The transformation of the coordinates leads to the new matrix **A′**, instead of **A**, in eq. (3). If **S** is the transformation matrix between the infinitesimal displacements around the equilibrium position

$$\begin{pmatrix} \delta R \\ \delta r \\ \delta\alpha \end{pmatrix} = \mathbf{S} \begin{pmatrix} \delta R_O \\ \delta R_4 \\ \delta R_5 \end{pmatrix}, \tag{18}$$

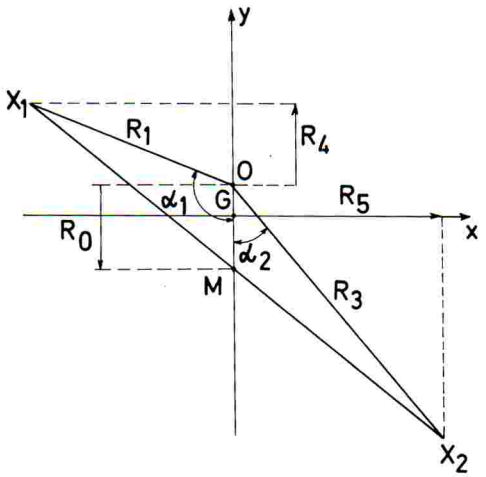

Fig. 5. Definition of the internal coordinates (R_O, R_4, R_5) for which $g^{1/2}$ is constant.

the **A′** matrix takes the form

$$\mathbf{A'} = \mathbf{S}^T\mathbf{A}\mathbf{S}. \tag{19}$$

6. Choice of matrix B

As stated in section 4, the matrix **B** [eq. (6)] is kept constant during the motion of the gaussians. This model is valid if, at any time, the potential energy can be truncated to a good approximation after the quadratic terms in the region covered by every gaussian. The easiest way to make this approximation valid is to consider thinner and thinner gaussian functions, i.e. to increase the value of **B**. Three values have been tested for the derivation of the autocorrelation function corresponding to the motion of the wavepacket on the adiabatic upper surface: **B** = 2**A′**, **B** = 3**A′** and **B** = 4**A′**. The result is not very sensitive to the value of **B**. Moreover, it has to be kept in mind that the quality of the basis set decreases when **B** increases. As a matter of fact, making the gaussians thinner worsens the expansion of $\Psi(q, 0)$ in this basis set [eq. (3)], because it becomes incomplete. The overlap integral $\int\int\int_{-\infty}^{\infty} g^{1/2}\,dq\;\Psi_0(q)\;\Psi(q, 0)$ is given in table 1 for three values of **B**. As a consequence, the size N [eq. (5)] of the basis set has to be increased, as illustrated by table 2. One can see that the basis set should contain at least sixty-six gaussian functions. However, since we intended to generate a whole set of autocorrelation functions with different conditions on the rotational quantum number J and on the diabatic potential, we restricted ourselves to $N = 30$ trajectories.

Table 1
Values of $I = \int\int\int_{-\infty}^{\infty} g^{1/2}\,dq\;\Psi_0(q)\;\Psi(q, 0)$ for H_2O^+ calculated with thirty trajectories for three values of **B** = n**A′**

n	I
2	0.9556
3	0.9154
4	0.8717

Table 2
Values of $I = \int\int\int_{-\infty}^{\infty} g^{1/2}\, dq\ \Psi_0(q)\ \Psi(q, 0)$ for H_2O^+ calculated with N trajectories, with $\mathbf{B} = 2\mathbf{A}'$

N	I
20	0.9080
30	0.9556
66	0.9950

7. Results

7.1. The adiabatic correlation function

7.1.1. Influence of J

As the upper adiabatic potential energy surface is already well known [8,9], we first study the influence of the quantum rotational number J on the autocorrelation function resulting from the motion of the wave packet on this surface, for both H_2O^+ and D_2O^+. Figs. 6 and 7 show the autocorrelation functions in the case where $J = 0$ [parts (a)] and $J = 10$ [parts (b)]. In both cases, the increase of J leads to a splitting of the first and second recurrences. As far as the first recurrence is concerned, this splitting is more important in the case of H_2O^+ than for D_2O^+, but one has to remember that at a given J the rotational energy is greater for H_2O than for D_2O. Thus one can conclude that the rotational excitation leads to qualitatively similar results in the adiabatic autocorrelation functions of H_2O^+ and D_2O^+ ($\tilde{B}\,^2A'/^2B_2$ state).

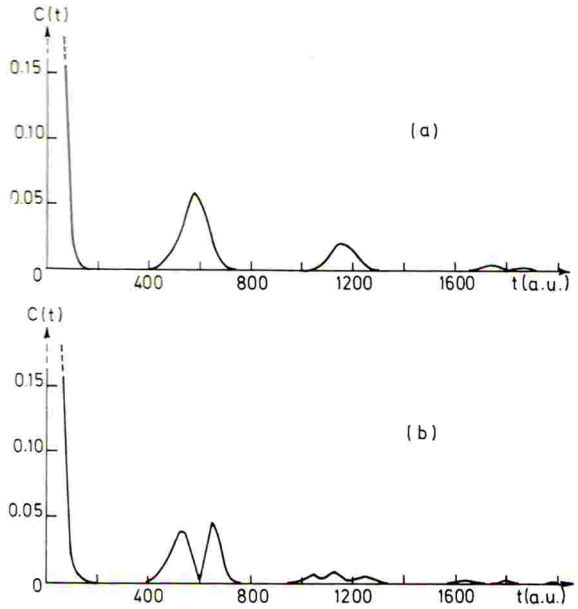

Fig. 6. Adiabatic calculated autocorrelation functions of H_2O^+ for two values of J: (a) $J = 0$ and (b) $J = 10$.

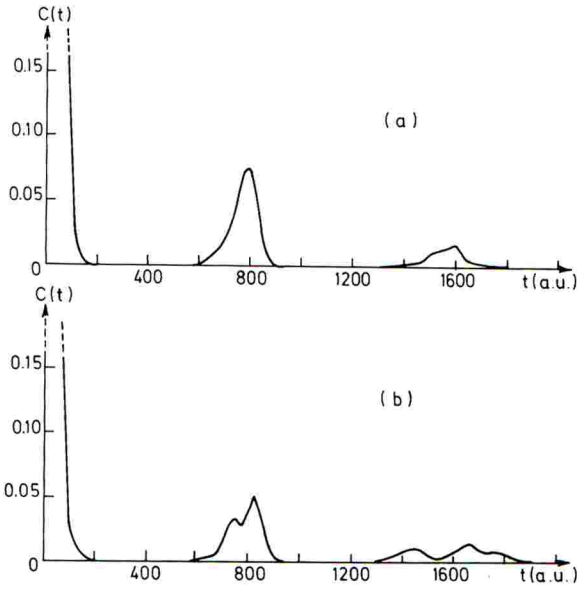

Fig. 7. Adiabatic calculated autocorrelation functions of D_2O^+ for two values of J: (a) $J = 0$ and (b) $J = 10$.

7.1.2. Isotope effect on the recurrence times

As far as the isotope effect is concerned, the comparison between parts (a) and (b) of fig. 1, or between fig. 6 and fig. 7 shows that it results in a displacement of the recurrences corresponding to the expected changes of the frequencies

$$T_{1\text{st rec}}(D_2O^+)/T_{1\text{st rec}}(H_2O^+) \approx 1.5.$$

7.1.3. Isotope effect on the transition probability and the correlation function

The heights of the first recurrences are slightly different (0.059 for H_2O^+, $J = 0$ and 0.075 for D_2O^+, $J = 0$). However, the probabilities of remaining on the adiabatic upper surface are equal to 0.101 and 0.066 respectively, i.e. H_2O^+ behaves more adiabatically than D_2O^+. This is in con-

tradistinction with the simple intuitive thinking based on the nuclear velocities in the coupling zone. As a matter of fact, as D_2O^+ is heavier, it moves then more slowly and, on this basis alone, its behavior is more adiabatic. However, the nuclear velocities are not the only variables in the expression of the Nikitin transition probability [12]. The impact parameter r_c [the value of the coordinate r when one passes through the seam $\alpha = \alpha_c(R)$] influences the value of p too. It has been shown [9] that this variable is in fact the factor which determines the value of p. In D_2O^+, the initial kinetic energy, i.e. the zero point energy, is lower than in H_2O^+, in particular that part in the antisymmetric mode r. As r is not excited in the photoexcitation process, the only possibility to increase its variation domain, i.e. the mean value of r_c, is the coupling with the other modes. This effect is expected to be more important after a rather long propagation time. However, as far as the motion on the adiabatic upper surface is concerned, this is not the case for the first passage in the coupling zone and one can consider (for the second passage too because the conditions have not changed very much [8,9]) that the coupling between the nuclear modes has no time to influence strongly the variation domain of r. Thus, the trajectories will pass nearer to the apex of the cone in D_2O^+ than in H_2O^+, inducing a stronger non-adiabatic transition to the lower adiabatic state, i.e. a more diabatic behavior.

The opposite isotope effect on the heights of the first recurrences and the probabilities gives evidence of the fact that the shape of the autocorrelation function is not only determined by the transition probability but depends also on the nuclear motion on the potential energy surface studied.

Fig. 1 (solid line) presents the experimental autocorrelation function, i.e. that obtained by Fourier transforming the third band of the photoelectron spectra of H_2O (fig. 1a) [22] and D_2O (fig. 1b) [23], compared with the calculated adiabatic autocorrelation function (dashed line) which is a weighted average of the autocorrelation functions obtained for $J = 0, 2, 5$ for H_2O^+ and $J = 0, 3, 5$ for D_2O^+. These values of J were chosen on the basis of the rotational distribution functions.

7.2. *The diabatic correlation function*

The existence of additional peaks, other than those coming from the adiabatic function, indicates that one part of the wave packet moves on a non-adiabatic potential energy surface and comes back to the Franck–Condon zone.

7.2.1. *Influence of the shape of the diabatic potential and influence of J*

Several diabatic potential energy surfaces have been tested. They all were obtained as explained in section 2. The first attempt results from 141 points calculated ab initio with the basis set and the CI matrix described in refs. [8,9]. The diabatic correlation functions (DCF) are presented in fig. 8. One an see that

$$T_{1\text{st rec}}(D_2O^+)/T_{1\text{st rec}}(H_2O^+) = 1575/1125 = 1.4.$$

The isotope shift of the recurrence is somewhat smaller than in the adiabatic case, but this effect can still be considered as a normal isotope effect.

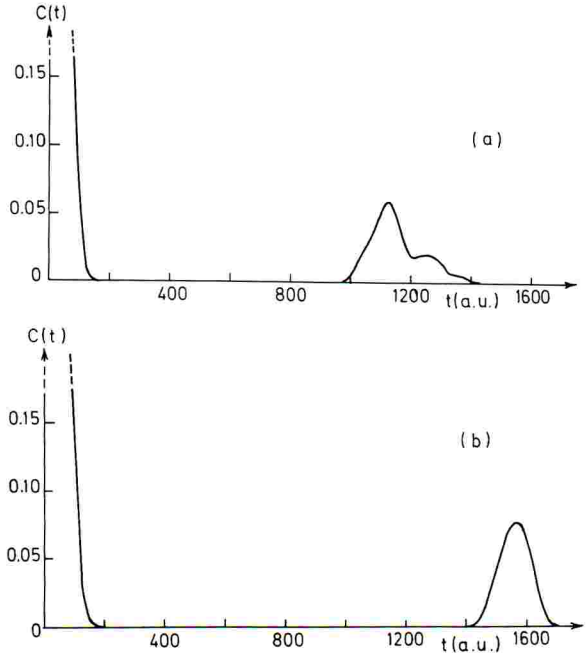

Fig. 8. Diabatic autocorrelation functions calculated with 141 ab initio points introduced in POT3: (a) H_2O^+, (b) D_2O^+. ($J = 5$.)

However, the recurrences do not appear in the expected time domain. Therefore, several attempts were made to study the influence of the curvature and the anharmonicity of the diabatic potential energy surface as well as the position of its minimum. This was done as follows. Let E_{AI} be the diabatic energies derived from ab initio calculations, E_c the diabatic energies resulting from a change in anharmonicity, curvature and position of the minimum (R_{eq}, 0, α_{eq}), and $(ds)^2$ the interval:

$$(ds)^2 = \sum_i \sum_j g_{ij} q_i q_j, \quad q_i = (R - R_{eq},\ r,\ \alpha - \alpha_{eq}),$$

where g_{ij} are the elements of the metric tensor.

$$E_c = E_{AI} + a(ds)^2 + b(ds)^3.$$

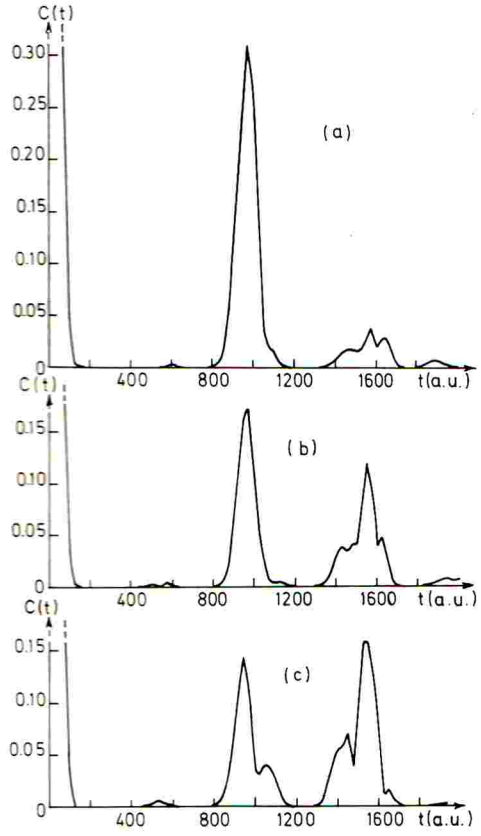

Fig. 9. Diabatic autocorrelation functions of H_2O^+ obtained with three different sets of parameters of $V^{(3)}(R_1, R_2, R_3)$ for $J = 2$.

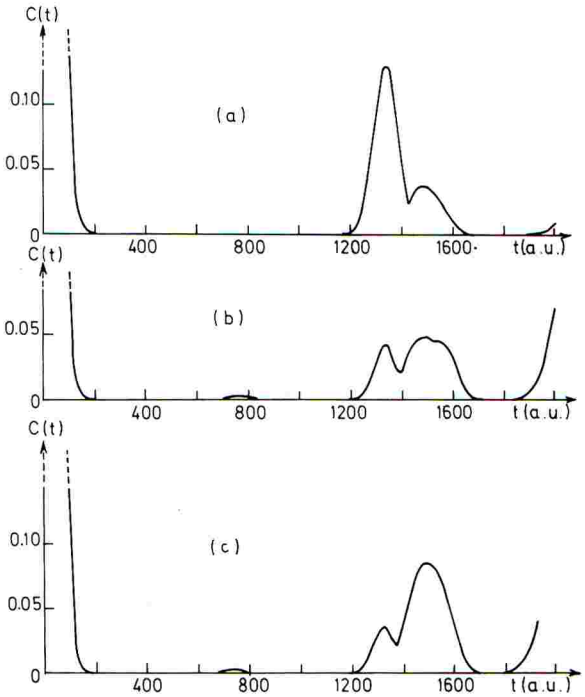

Fig. 10. Diabatic autocorrelation functions of D_2O^+ obtained with three different sets of parameters of $V^{(3)}(R_1, R_2, R_3)$ for $J = 3$.

The variation of a and b leads to different sets of energies E_c. The new values of E_c are then introduced as parameters in POT3 and a new expression for $V(R, r, \alpha)$ results. The best correlation functions obtained, as far as the positions of the diabatic recurrences are concerned, are shown in figs. 9 and 10 for the values of J corresponding to the maximum of the rotational distribution functions. In all the other calculated cases, the recurrence times were worse and the heights varied very much depending on the potential used. An increase in J results in a decrease in the first recurrence in the DCF of H_2O^+ and a change in the shape of the second one. The latter is composite and the variation of J has different influences on the components of the recurrence. This is also the case for the two components of the first recurrence of D_2O^+. The weighted average on J of the DCFs is presented in fig. 11.

7.2.2. Comparison with experiments and isotope effects

Let us compare fig. 11 with fig. 1. In the case of

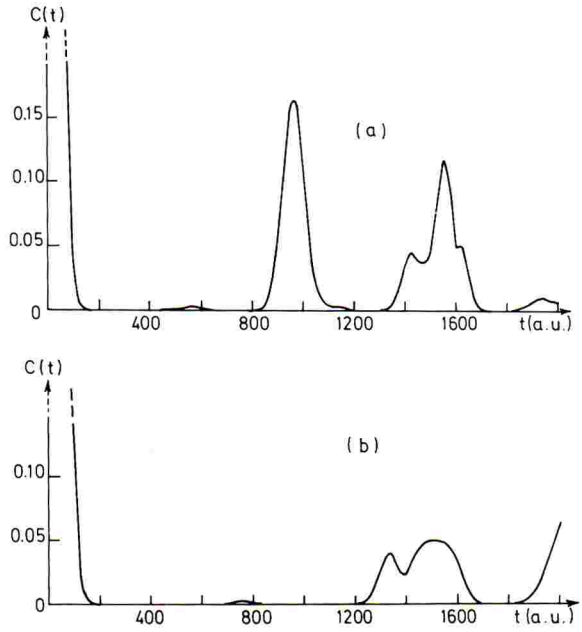

Fig. 11. Weighted average on J of the diabatic autocorrelation functions corresponding to case (b) of figs. 9 and 10: (a) H_2O^+, (b) D_2O^+.

H_2O^+, (fig. 11a) one obtains a calculated DCF with two recurrences, the first one at $t = 975$ au (DCF = 0.163) and the second one for $1300 \lesssim t \lesssim 1700$ ($t_{max} \approx 1550$ au, DCF = 0.118). The first one is a single peak while the second one is composite. If one considers the experimental function in fig. 1a, the first non-adiabatic recurrence takes place at $t = 900$ au with a height of 0.083. A small secondary peak is observed at $t = 1000$ au which can be reproduced in only few of the calculated correlation functions (fig. 9). The second non-adiabatic recurrence is very weak (≈ 0.02). It occurs at $1225 < t < 1500$ au and is composite. The relative errors on the recurrence times are respectively 8% (first recurrence) and 14% (second one). However, the most important discrepancies concern the heights of the recurrences, particularly the second one. In the experimental autocorrelation function, it is very weak but this cannot be accounted for in any of the diabatic correlation functions calculated here. However, one has to keep in mind that one neglected the interference term between the adiabatic and diabatic wave packets. This term contains the square root of the corresponding populations multiplied by the overlap integral between the two wave packets. In the very improbable case where they nearly coincide, the interference term is of the order of 0.2–0.3. These high values are weighted by the overlap integral which lowers them down. However, the interference term may be sufficiently important to cancel a part of the autocorrelation function out as well as to increase it.

In the case of D_2O^+, only the first recurrence appears in the time domain considered. It has two components, in the calculated function as well as in the experimental one. The time values corresponding to the two maxima are $t_1 = 1350$ au, $t_2 = 1500$ au for the calculated curve and $t_1 = 1220$ au, $t_2 = 1500$ au for the experimental one, i.e. relative errors of 10% and less than 2% respectively. As far as the heights are concerned, one obtains $h_1 = 0.039$, $h_2 = 0.049$ in fig. 11b and $h_1 = 0.055$, $h_2 = 0.049$ in fig. 1b. The agreement between the calculated and experimental correlation functions is somewhat better in the case of D_2O^+ than in the case of H_2O^+.

Quantitatively, the DCF is not well reproduced in the case of H_2O^+ as far as the heights of the function are concerned. However, qualitatively, one can consider that the results are not too bad if one takes into account firstly that the nuclear motion on the diabatic surface involves very distorted geometries and will be very sensitive to the shape of the surface at these geometries, and secondly that the neglected interference term may be important. As a matter of fact, we emphasize that the isotope effect is rather well accounted for in the calculated DCF: the first recurrence is a single peak in the case of H_2O^+ whereas it has two components in the case of D_2O^+. In the case of H_2O^+, all of the trajectories which come back near the Franck–Condon zone do so at $t \approx 975$ au, whereas for D_2O^+, some of them come back around $t \approx 1350$ au and some others around $t \approx 1500$ au.

8. Discussion

8.1. Isotope effect on the shape of the first diabatic recurrence

In the case of D_2O^+, a detailed analysis of the trajectories reveals that those for which the recur-

rence time is ≈ 1500 au are all characterized by a great percentage of internal energy in the antisymmetric mode r. Our explanation of such different behavior in D_2O^+ and H_2O^+ rests on the difference in the variation of the coefficients in the expression for the kinetic energy. In order to simplify somewhat the discussion, we consider only the expression for the vibrational kinetic energy, T_{shape} [21]. For the general nuclear framework XOX represented by the coordinates (R, r, α), one has

$$T_{\text{shape}} = m_X \sum_i \sum_j t_{ij} \dot{q}_i \dot{q}_j$$
$$= m_X \left(t_{11} \dot{R}^2 + t_{22} \dot{r}^2 + t_{33} \dot{\alpha}^2 + 2t_{13} \dot{\alpha} \dot{R} + 2t_{23} \dot{\alpha} \dot{r} \right). \quad (20)$$

If the coefficients t_{ij} are not functions of m_X, then (20) can be replaced by

$$T_{\text{shape}} = \sum_i \sum_j t_{ij} \dot{q}_{i,M} \dot{q}_{j,M}, \quad (21)$$

where the coordinates $q_{i,M}$ are mass weighted

$$q_{i,M} = m_X^{1/2} q_i, \quad q_i = R, r, \alpha.$$

The expression for T_{shape} is invariant in m_X. Thus, a variation of m_X will change all the velocities $\dot{q}_i$ by the same factor. However, if the coefficients t_{ij} are distinct functions of m_X, expression (21) is no longer invariant in the mass m_X. Then, isotopic substitution will not only speed up (or slow down) the trajectories, but can also completely modify them. The expressions for the t_{ij} are:

$$t_{11} = 1 - 2\gamma \cos^2(\alpha/2),$$
$$t_{22} = \tfrac{1}{4}\left[1 - 2\gamma \sin^2(\alpha/2)\right],$$
$$t_{33} = \tfrac{1}{4}\left\{ R^2 \left[1 - 2\gamma \sin^2(\alpha/2)\right] + \tfrac{1}{4} r^2 \left[1 - 2\gamma \cos^2(\alpha/2)\right] \right\},$$
$$t_{13} = \tfrac{1}{2}\gamma R \sin \alpha,$$
$$t_{23} = -\tfrac{1}{8}\gamma r \sin \alpha,$$
$$\gamma = m_X/(m_O + 2m_X).$$

The variation of the dynamical couplings ($i \neq j$) as a function of m_X ($\div\gamma$) is stronger than that of the diagonal terms ($\div[1 - 2\gamma \ldots]$). This may explain the differences in the behavior of H_2O^+ and D_2O^+.

8.2. Isotope effect on the probabilities of remaining on the potential energy surface

The populations of being still on the diabatic surface at the first recurrence times are presented in table 3. These results apparently suggest that the behavior of D_2O^+ is less diabatic than that of H_2O^+. This seems to disagree with the calculated probabilities of remaining on the adiabatic surface (section 7.1.3). In a first step, one has calculated the population on the adiabatic upper state. This population is represented in fig. 3 by contributions 1 and 3. As (1 + 3) is greater for H_2O^+ than for D_2O^+, contributions 2 and 4 are more important for the deuterated system. Then, one expects contributions (5 + 7) to be greater for the heavier ion. However, one obtains the inverse result. Our explanation is as follows. The flux of trajectories nr. 2 is identical with the flux nr. 5, i.e. flux 5 is more important in D_2O^+ than in H_2O^+. The trajectories that make up this flux follow a very anharmonic potential energy surface which allows very important distortions of the nuclear framework. Furthermore, the dynamical couplings are stronger for D_2O^+ than for H_2O^+. When the trajectories of the D_2O^+ system come back (flux 7) in the coupling zone, the impact parameter r will take larger values, inducing a more adiabatic behavior, i.e. flux 7 is much less important than flux 5.

8.3. Relation between P(t) and C(t)

As far as the heights of the peaks are concerned, they are calculated to be lower for D_2O^+ than for H_2O^+, in agreement with the experimental results. This is at first sight rather surprising if one considers the population P which is still on the diabatic surface (which coincides with the

Table 3
Population P on the diabatic surface for the values of t corresponding to the first recurrence

Isotope species	t (au)	P
H_2O^+	975	0.85
D_2O^+	1350	0.83
D_2O^+	1500	0.80

upper adiabatic one in the Franck–Condon zone) for the recurrence times (cf table 3). The great differences between the values of the remaining population and the DCF prove that the motion of the nuclei on the surface is the leading factor determining the heights of the peaks in the autocorrelation function, rather than the transition probability. This has already beeen pointed out by Köppel [3] in the case of $C_2H_4^+$. Therefore, it is somewhat dangerous to derive a rate constant for a non-adiabatic transition process from an autocorrelation function [24].

8.4. *Coupling with rotation*

The motion on the diabatic potential energy surface leads to very strong distortions of the nuclear framework so that a rather small percentage of the wave packet comes back in the Franck–Condon zone. Furthermore, these large deformations are subject to coupling with the rotation. The importance of this coupling depends on the shape of the diabatic surface for small values of the coordinate α. If the surface is not very steep along this coordinate when the molecule is highly distorted (in the sense $R_1 \gg R_3$) the bending motion can transform into internal rotation of the fragment OX_2 (cf fig. 12a). If the potential is very steep for small values of α, the bending motion cannot transform into internal rotation (fig. 12b). This explains why the influence of rotation on the vibrational motion of the nuclei, i.e. the shape of the correlation function versus J, can vary according to the characteristics of the potential energy surface.

Finally, we note that this influence of J in the correlation function has nothing to do with the rotational correlation function due to the overall rotation of the body-fixed reference frame. The experimental functions have already been corrected for this rotational part [1]. The expressions for the initial wavefunction [eqs. (2) and (3)] and the gaussians [eq. (6)] involve only the three vibrational coordinates. Their variations as a function of time are influenced more or less strongly by the rotation of the system. Therefore, what has been studied here is the importance of Coriolis interaction on the vibrational correlation function.

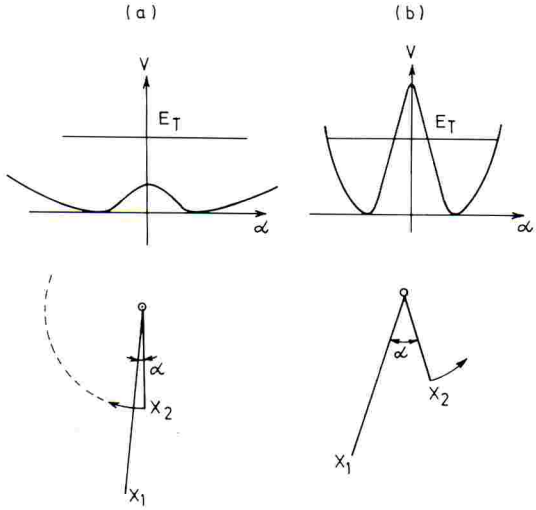

Fig. 12. The distorted molecule and the possible (a) or impossible (b) internal rotation motion of OX_2, according to the shape of the potential V and the total energy E_T.

9. Conclusions

The purpose of this work is to study the isotope effect observed in the autocorrelation function of H_2O^+ and D_2O^+ in their $\tilde{B}\,^2B_2/^2A'$ state. This state is coupled to the $\tilde{A}\,^2A_1/^2A'$ state via a conical intersection [7–9]. The method used in this work consists in splitting the set of trajectories into two parts: one moving on the adiabatic surface associated with the upper cone (fig. 2), and a second part associated with the trajectories moving on the diabatic surface H_{11} (fig. 4). Both parts were assumed to give rise to independent correlation functions which were simply added, i.e. interference effects were disregarded.

The adiabatic correlation functions agree qualitatively with the experimental ones (fig. 1). If one compares fig. 11 with fig. 1, one sees that the agreement between the diabatic autocorrelation functions and the experimental ones is qualitatively good as far as the recurrence times are concerned, but not very satisfactory for the calculated heights which are too large, which can be due to the neglect of the interference term. However, the isotope effect is satisfactorily reproduced. The first diabatic recurrence in H_2O^+ is calculated to be single peaked whereas that in D_2O^+ is

composite. In the case of H_2O^+, all trajectories that come back near the Franck–Condon zone do so at a time ≈ 975 au. In the case of D_2O^+, the trajectories which come back near the Franck–Condon zone are divided into two sets. The first set of trajectories comes back at ≈ 1350 au, the other does so at ≈ 1500 au. Our explanation of such different behavior in D_2O^+ and H_2O^+ rests on the fact that the coefficients of the velocity products in T_{shape} are distinct functions of m_X and that the dynamical couplings are greater for the heavier system.

The nuclear motion is also seen to be responsible for the great difference between the probability of being still on the diabatic potential energy surface at the recurrence times (≈ 0.8) and the heights of the first recurrences. A somewhat similar situation has already been encountered by Köppel [3] in the $C_2H_4^+$ system. As a matter of fact, the nuclear framework can distort very strongly when the motion takes place on the diabatic potential energy surface and only a small number of trajectories do come back in the Franck–Condon zone. Thus, the rate constant which we calculated for the depopulation of the upper adiabatic $^2A'$ state of H_2O^+ via the conical intersection only reflects the evanescence of WP1 but tells us nothing about WP2, which comes back on the upper adiabatic potential surface with a probability of 0.8 after one period. Therefore, the large calculated value of 10^{14} s^{-1} for the rate constant [8,9] characterizing the depopulation of the upper adiabatic state of H_2O^+ has to be reinterpreted and corrected by taking into account that part of the diabatic wave packet WP2 which comes back on the upper adiabatic surface. This high calculated value of 10^{14} s^{-1} [8,9] gives evidence that fluxes 2 and 4 (see fig. 3) are important. However, flux nr. 2 (= nr. 5) comes back on the upper adiabatic state (flux 7). If the probability that WP2 returns to the upper adiabatic surface (flux 7) after one period ranges from 0.8 to 0.85 (to which 5% has to be added coming from WP1: flux 3), one can estimate the relaxation rate constant (corresponding to fluxes 4 and 8) to be of the order of 5×10^{12} s^{-1}, i.e. the population of the upper adiabatic state has dropped down to 50% after five or six vibrational periods. Thus, this correction coming from WP2 cannot be neglected since it lowers considerably the order of the relaxation rate constant.

Acknowledgement

I would like to express my gratitude to Professor J.C. Lorquet for stimulating discussions and several comments that led to significant improvement in the manuscript. I wish to thank Dr. A.J. Lorquet for very helpful and interesting discussions and I am grateful to Drs. A.J. Lorquet, J. Delwiche, M.J. Hubin-Franskin and Mr B. Leyh for providing me with experimental correlation functions of H_2O^+ and D_2O^+. This work has been supported by the Belgian Government (Action de Recherche Concertée) and the "Fonds de la Recherche Fondamentale Collective".

Appendix: Overlap integral between two gaussian functions in a three-dimensional case

Let us consider the three coordinates u, v, w, components of the vector

$$\boldsymbol{q} = \begin{pmatrix} u \\ v \\ w \end{pmatrix}, \tag{A.1}$$

and the two gaussian functions $G_i(\boldsymbol{q})$, $G_j(\boldsymbol{q})$:

$$\begin{aligned} G_i(\boldsymbol{q}) &= N_i \exp\left[-(1/2\hbar)(\boldsymbol{q}-\boldsymbol{q}_i)^{\mathrm{T}} \cdot \mathbf{A}(\boldsymbol{q}-\boldsymbol{q}_i) + (\mathrm{i}/\hbar)\boldsymbol{p}_i^{\mathrm{T}} \cdot (\boldsymbol{q}-\boldsymbol{q}_i)\right], \\ G_j(\boldsymbol{q}) &= N_j \exp\left[-(1/2\hbar)(\boldsymbol{q}-\boldsymbol{q}_j)^{\mathrm{T}} \cdot \mathbf{B}(\boldsymbol{q}-\boldsymbol{q}_j) + (\mathrm{i}/\hbar)\boldsymbol{p}_j^{\mathrm{T}} \cdot (\boldsymbol{q}-\boldsymbol{q}_j)\right], \end{aligned} \tag{A.2}$$

where the superscript T denotes the transposed vector and **A** and **B** are two distinct real matrices.

The overlap integral between G_i and G_j is

$$S_{ji} = \iiint_{-\infty}^{\infty} g^{1/2}\, \mathrm{d}u\, \mathrm{d}v\, \mathrm{d}w\, G_j^*(\boldsymbol{q})\, G_i(\boldsymbol{q}), \tag{A.3}$$

where g is the determinant of the metric tensor $\mathbf{g}$ corresponding to the coordinates $\boldsymbol{q}$, and $(g^{1/2}\, \mathrm{d}u\, \mathrm{d}v\, \mathrm{d}w)$ is the invariant elementary volume. In the following, the symbol $\iiint_{-\infty}^{\infty}$ will be simplified into $\int$ and the product $\mathrm{d}u\, \mathrm{d}v\, \mathrm{d}w$ will be represented by $\mathrm{d}\boldsymbol{q}$. A part of the integrand of (A.3) can be taken out of the symbol $\int$:

$$S_{ji} = N_i N_j \exp\left[-(1/\hbar)(\boldsymbol{q}_i - \boldsymbol{q}_j)^{\mathrm{T}} \cdot \mathbf{D}(\boldsymbol{q}_i - \boldsymbol{q}_j) + K + (\mathrm{i}/\hbar)\left(\boldsymbol{p}_j^{\mathrm{T}} \cdot \boldsymbol{q}_j - \boldsymbol{p}_i^{\mathrm{T}} \cdot \boldsymbol{q}_i\right)\right] I_{ji}, \tag{A.4}$$

where

$$I_{ji} = \int \left(g^{1/2}\, \mathrm{d}\boldsymbol{q}\right) \exp\left[-(1/\hbar)(\boldsymbol{q} - \boldsymbol{Q}_{ji})^{\mathrm{T}} \cdot \mathbf{C}(\boldsymbol{q} - \boldsymbol{Q}_{ji}) + (\mathrm{i}/\hbar)(\boldsymbol{p}_i - \boldsymbol{p}_j)^{\mathrm{T}} \cdot \boldsymbol{q}\right],$$

$$(\mathbf{D})_{\alpha\beta} = D_{\alpha\beta} = A_{\alpha\beta} B_{\alpha\beta} / 2\left(A_{\alpha\beta} + B_{\alpha\beta}\right), \tag{A.5}$$

$$C_{\alpha\beta} = \tfrac{1}{2}\left(A_{\alpha\beta} + B_{\alpha\beta}\right), \tag{A.6}$$

$$\boldsymbol{Q}_{ji} = \mathbf{C}^{-1}\boldsymbol{b} = \mathbf{C}^{-1}\begin{pmatrix} b_1 \\ b_2 \\ b_3 \end{pmatrix}, \tag{A.7}$$

$$b_i = C_{1i} X_{i1} + C_{2i} Y_{i2} + C_{3i} Z_{i3}, \tag{A.8}$$

$$X_{\alpha\beta} = \left(A_{\alpha\beta} u_i + B_{\alpha\beta} u_j\right) / \left(A_{\alpha\beta} + B_{\alpha\beta}\right), \tag{A.9a}$$

$$Y_{\alpha\beta} = \left(A_{\alpha\beta} v_i + B_{\alpha\beta} v_j\right) / \left(A_{\alpha\beta} + B_{\alpha\beta}\right), \tag{A.9b}$$

$$Z_{\alpha\beta} = \left(A_{\alpha\beta} w_i + B_{\alpha\beta} w_j\right) / \left(A_{\alpha} + B_{\alpha\beta}\right), \tag{A.9c}$$

$$K = C_{11} X_{11}^2 + C_{22} Y_{22}^2 + C_{33} Z_{33}^2 + 2C_{12} X_{12} Y_{12} + 2C_{13} X_{13} Z_{13} + 2C_{23} Y_{23} Z_{23} - \boldsymbol{Q}_{ji}^{\mathrm{T}} \cdot \mathbf{C}\boldsymbol{Q}_{ji}. \tag{A.10}$$

If one performs a transition of the coordinates

$$\boldsymbol{\mathcal{R}} = \boldsymbol{q} - \boldsymbol{Q}_{ji},$$

then

$$I_{ji} = \int \left(g^{1/2}\, \mathrm{d}\boldsymbol{\mathcal{R}}\right) \exp\left[-(1/\hbar)\boldsymbol{\mathcal{R}}^{\mathrm{T}} \cdot \mathbf{C}\boldsymbol{\mathcal{R}} + (\mathrm{i}/\hbar)(\boldsymbol{p}_i - \boldsymbol{p}_j)^{\mathrm{T}} \cdot (\boldsymbol{\mathcal{R}} + \boldsymbol{Q}_{ji})\right]. \tag{A.11}$$

Let us diagonalize $\mathbf{C}$ by a unitary transformation $\mathbf{S}$:

$$\mathbf{T} = \mathbf{S}\mathbf{C}\mathbf{S}^{-1}. \tag{A.12}$$

The new coordinates and momenta are given by

$$\boldsymbol{V} = \mathbf{S}\boldsymbol{\mathcal{R}}, \quad \boldsymbol{p}_V = \mathbf{S}^{-1}\boldsymbol{p}. \tag{A.13}$$

for which the new metric tensor $\mathbf{g}'$ has the same determinant as $\mathbf{g}$ since the matrix transformation is unitary, i.e. the elementary volume $(g^{1/2}\, \mathrm{d}\boldsymbol{\mathcal{R}})$ becomes $(g^{1/2}\, \mathrm{d}\boldsymbol{V})$.

$$I_{ji} = \int \left(g^{1/2}\, \mathrm{d}\boldsymbol{V}\right) \exp\left[-(1/\hbar)\boldsymbol{V}^{\mathrm{T}} \cdot \mathbf{T}\boldsymbol{V} + (\mathrm{i}/\hbar)(\boldsymbol{p}_{V_i} - \boldsymbol{p}_{V_j})^{\mathrm{T}} \cdot (\boldsymbol{V} + \boldsymbol{V}_{ji})\right]. \tag{A.14}$$

As the **T** matrix is diagonal, if g is a constant, the three-dimensional integral becomes a product of three one-dimensional integrals that have well-known expressions [25]. One finally obtains

$$I_{ji} = g^{1/2}(\pi^3\hbar^3/\det \mathbf{T})^{1/2} \exp\left[-(1/4\hbar)(\boldsymbol{p}_{V_i} - \boldsymbol{p}_{V_j})^{\mathrm{T}} \cdot \mathbf{T}^{-1}(\boldsymbol{p}_{V_i} - \boldsymbol{p}_{V_j}) + (\mathrm{i}/\hbar)(\boldsymbol{p}_{V_i} - \boldsymbol{p}_{V_j})^{\mathrm{T}} \cdot \boldsymbol{V}_{j_i}\right]. \quad \text{(A.15}$$

If one comes back to the initial coordinates $\boldsymbol{q}$, one has

$$I_{ji} = g^{1/2}(\pi^3\hbar^3/\det \boldsymbol{C})^{1/2} \exp\left[-(1/4\hbar)(\boldsymbol{p}_i - \boldsymbol{p}_j)^{\mathrm{T}} \cdot \mathbf{C}^{-1}(\boldsymbol{p}_i - \boldsymbol{p}_j) + (\mathrm{i}/\hbar)(\boldsymbol{p}_i - \boldsymbol{p}_j)^{\mathrm{T}} \cdot \boldsymbol{Q}_{ji}\right]. \quad \text{(A.16)}$$

References

[1] A.J. Lorquet, J.C. Lorquet, J. Delwiche and M.J. Hubin-Franskin, J. Chem. Phys. 76 (1982) 4692.

[2] M. Bixon and J. Jortner, J. Chem. Phys. 77 (1982) 4175;
D. Dehareng, B. Leyh, M. Desouter-Lecomte, J.C. Lorquet, J. Delwiche and M.J. Hubin-Franskin, J. Chem. Phys. 79 (1983) 3719;
J. Brickmann, J. Chem. Phys. 78 (183) 1884;
T. Kakitani, Chem. Phys. Letters 109 (1984) 488;
V.B. Pavlov-Verevkin, Chem. Phys. 98 (1985) 361.

[3] H. Köppel, Chem. Phys. 77 (1983) 359.

[4] E.J. Heller, J. Chem. Phys. 75 (1981) 2923.

[5] D. Dehareng, Chem. Phys. 84 (1984) 393.

[6] E.J. Heller, J. Chem. Phys. 65 (1976) 4979;
K.C. Kulander and E.J. Heller, J. Chem. Phys. 69 (1978) 2439;
D.J. Tannor and E.J. Heller, J. Chem. Phys. 77 (1982) 202,
R.T. Skodje, Chem. Phys. Letters 109 (1984) 227.

[7] G.G. Balint-Kurti and R.N. Yardley, Chem. Phys. Letters 36 (1975) 342;
C.F. Jackels, J. Chem. Phys. 72 (1980) 4873.

[8] D. Dehareng, X. Chapuisat, J.C. Lorquet, C. Galloy and G. Raseev, J. Chem. Phys. 78 (1983) 1246.

[9] D. Dehareng, These de doctorat, Université de Liège, Belgium (1983).

[10] E.J. Heller, J. Chem. Phys. 68 (1978) 2066, 3891.

[11] C. Leforestier, Chem. Phys. Letters 51 (1977) 132.

[12] E.E. Nikitin, Chemische Elementarprozesse, ed. H. Hartmann (Springer, Berlin, 1968) p. 70;
E.E. Nikitin, Theory of elementary atomic and molecular processes in gases (Clarendon Press, Oxford, 1974);
E.E. Nikitin and L. Zülicke, Selected topics of the theory of chemical elementary processes (Springer, Berlin, 1978);
M. Desouter-Lecomte, C. Galloy, J.C. Lorquet and M. Vaz Pires, J. Chem. Phys. 71 (1979) 3661.

[13] A.D.Mc Lachlan, Mol. Phys. 4 (1961) 417;
M. Baer, Chem. Phys. Letters 35 (1975) 112; Chem. Phys. 15 (1976) 49;
C.A. Mead and D.G. Truhlar, J. Chem. Phys. 77 (1982) 6090.

[14] M. Desouter-Lecomte, D. Dehareng and J.C. Lorquet, J. Chem. Phys., submitted for publication.

[15] Program POT 3, University of Reading, USA.

[16] K.S. Sorbie and J.N. Murrell, Mol. Phys. 29 (1975) 1387.

[17] J.N. Murrell, S. Carter and I.M. Mills, Mol. Phys. 37 (1979) 1885;
J.N. Murrell, S. Carter, I.M. Mills and M.F. Guest, Mol. Phys. 42 (1981) 605;
S. Carter and J.N. Murrell, J. Phys. Chem. 88 (1984) 4887.

[18] E. Wigner, Phys. Rev. 40 (1932) 749.

[19] R.J. Bartlett, I. Shavitt and G.D. Purvis, J. Chem. Phys. 71 (1979) 281.

[20] M.J. Davis and E.J. Heller, J. Chem. Phys. 71 (1979) 3383;
E.J. Heller, J. Chem. Phys. 65 (1976) 4999; 67 (1977) 3339.

[21] X. Chapuisat, A. Nauts and G. Durand, Chem. Phys. 56 (1981) 91.

[22] B. Leyh, Mémoire de fin d'étude (Université de Liège, Liège 1982).

[23] A.J. Lorquet, J. Delwiche, M.J. Hubin-Franskin, unpublished results.

[24] J.E. Pollard, D.J. Trevor, J.E. Reutt, Y.T. Lee and D.A. Shirley, J. Chem. Phys. 81 (1984) 5302.

[25] I.S. Gradshteyn and I.M. Ryzhik, Tables of integrals, series and products (Academic Press, New York, 1965).